Journal of Nuclear Materials 390–391 (2009) 1005–1008

Contents lists available at ScienceDirect

Journal of Nuclear Materials

journal homepage: www.elsevier.com/locate/jnucmat

Mass changes in NSTX surface layers with Li conditioning as measured by quartz microbalances

C.H. Skinner [a,*], H.W. Kugel [a], A.L. Roquemore [a], P.S. Krstic [b], A. Beste [b]

[a] Princeton Plasma Physics Laboratory, P.O. Box 451, Princeton, NJ 08543, USA
[b] Oak Ridge National Laboratory, Oak Ridge, TN 37831, USA

ARTICLE INFO

PACS:
52.40.Hf
52.90.+z

ABSTRACT

Dynamic retention of deuterium, lithium deposition, and the stability of thick deposited layers were measured by three quartz crystal microbalances (QMB) deployed in plasma shadowed areas at the upper and lower divertor and outboard midplane in the National Spherical Torus Experiment (NSTX) that was equipped with a lithium evaporator. Deposition of 185 μg/cm^2 over 3 months in 2007 was measured by a QMB at the lower divertor while a QMB on the upper divertor, that was shadowed from the evaporator, received an order of magnitude less deposition. During helium glow discharge conditioning both neutral gas collisions and the ionization of lithium and subsequent drift of the ion interrupted the lithium deposition on the lower divertor. We present calculations of the relevant mean free paths. Occasionally strong variations in the QMB frequency of thick lithium films were observed suggesting relaxation of mechanical stress and/or flaking or peeling of the deposited layers.

1. Introduction

Lithium as a plasma facing material offers reduced recycling of hydrogenic species and the potential for withstanding high heat and neutron fluxes in fusion reactors [1]. Lithium evaporations of a few mg up to 1 g have been applied between discharges in the National Spherical Torus Experiment (NSTX) [2] by an oven that directed a collimated stream of lithium vapor toward the graphite tiles of the lower center stack and divertor. Significant benefits to the performance of divertor plasmas in both L-and H-mode confinement regimes heated by high-power neutral beams were observed [3–6].

Quartz crystal microbalances (QMBs) have been used to monitor deposition of eroded materials in tokamaks [7] and study deposition and dynamic retention in NSTX [8,9]. Before plasma operations the crystals were exposed to the vessel bakeout at 350 °C for several days. During this time room temperature air was blown through the QMB cooling lines and kept the QMB temperature to below 150 °C. During the campaign the vessel was periodically boronized using a glow discharge of 10% trimethyl boron $B(CD_3)_3$ and 90% helium [10].

The increase in pulse duration and intensity of plasma wall interactions in next step devices such as ITER will lead to increased erosion of plasma facing materials and concomitant deposition of these materials in layers of unprecedented thickness on internal components. It is well known that thick films can detach from a substrate due to mechanical stress and differential thermal expansion. In a fusion device such detachment will lead to the generation of flakes and dust containing material from plasma facing components and/or tritium. These can either be transported to the plasma core potentially contaminating it with high Z material [11] or fall into inaccessible areas and complicate efforts to control the tritium and dust inventory [12–14]. Lithium coatings on the NSTX QMB crystals grow to be of micron scale and exhibit fluctuations in apparent mass that appear to be due to mechanical instabilities. We report real time measurements of lithium deposition in vacuum and during glow discharges and on the mechanical stability of thick deposited layers.

2. Lithium deposition during He glow discharge

In 2007 a LiThium EvaporatoR (LiTER) was located at the upper port at bay F and directed lithium vapor toward the graphite tiles of the lower center stack and divertor to control recycling. The evaporation was continued during intershot helium glow discharge conditioning (HeGDC) as the cool down time of the evaporator was much longer than the intershot interval. The QMBs recorded the deposition in line-of-sight and in areas shadowed from the evaporator at the locations shown in Fig. 1. The distance from LiTER to the upper, midplane and lower QMBs was 1.04, 2.48 and 3.17 m, respectively. The upper and lower QMBs were located in 7 cm wide slots in the upper and lower outer divertor, 7 cm back from the plasma facing tile surface. The frequency constant of the

* Corresponding author. Tel.: +1 609 243 2214; fax: +1 609 243 2665.
E-mail address: cskinner@pppl.gov (C.H. Skinner).

0022-3115/$ - see front matter © 2009 Elsevier B.V. All rights reserved.
doi:10.1016/j.jnucmat.2009.01.263

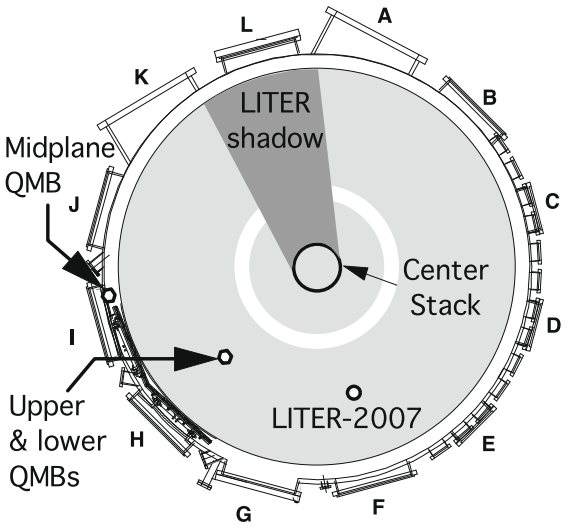

Fig. 1. Top view of the NSTX vessel with center stack, location of the LiTER evaporator and the QMBs. The major radius of the vessel wall is 1.7 m.

AT cut crystal quoted by the manufacturer is 166,100 Hz cm and the sensitivity was confirmed by ion beam analysis [8]. Ref. [9] contains more details on the QMBs and their geometry.

Before lithium evaporation the QMBs showed a transient rise in mass due to dynamic retention of deuterium at the time of the plasma discharge followed by a slow decay as reported previously [9]. During lithium evaporation these transients were superposed on an upward slope due to the lithium deposition on the lower divertor. During the prefill and post-discharge phase of a shot, vessel pressures are in the 10^{-4} torr range. At these elevated pressures lithium transport changes from molecular flow to the viscous flow regime so that lithium can diffuse to regions that are shadowed from a direct line-of-sight to the evaporator. Fig. 2 shows the effect of a gas-only pulse (without plasma) that filled the vessel with 1.3 mtorr (0.18 Pa) of deuterium and interrupted the deposition on the lower Bay H QMB while the upper Bay H QMB, that was out of line-of-sight of the evaporator and that previously did not show a rise, now indicates a small rise in mass. Deposition on the lower QMB resumed about a minute later during the pump out when the lithium mean free path approached the dimensions of the NSTX vacuum chamber.

The mean free path (λ_1) of neutral lithium in molecular deuterium was calculated from the momentum transfer scattering cross section (σ_{12}) using the formalism in Ref. [15] for a multicomponent gas. The cross sections were calculated on basis of highly accurate calculations of LiH ground singlet ($X^1\Sigma^+$) and triplet ($a^3\Sigma^+$) potential curves, using coupled cluster singles–doubles–triples–quadruples (CCSDTQ) method with unrestricted Hartree-Fock [16], equivalent to the full configuration interaction for the four-electron systems, and are in good agreement with the full valence CI calculations of Boutalib et al. [17]. Fully quantum–mechanical calculations of the cross sections, convergent in partial waves, were performed in the range 10^{-4}–0.12 eV, using Johnson method of logarithmic derivatives [18,19] and applying plane-wave boundary conditions for nuclear motion at R_{max} = 100 Bohrs. The singlet and triplet potentials were smoothly matched to the asymptotic van der Walls form [20]. The calculated mean free path of Li at 627 °C in a hypothetical atmosphere of 1 mtorr (0.13 Pa) of atomic deuterium at 27 °C is 3.94 cm. The momentum transfer cross section of lithium on molecular deuterium was estimated from Li + D cross section using analogy with comparison of fully quantal results of H + D and H + D_2 in Refs. [18,19]. The mean free path of Li at 627 °C in 1 mtorr of molecular deuterium at 27 °C is estimated to be 7.7 cm and varies inversely with the D_2 pressure.

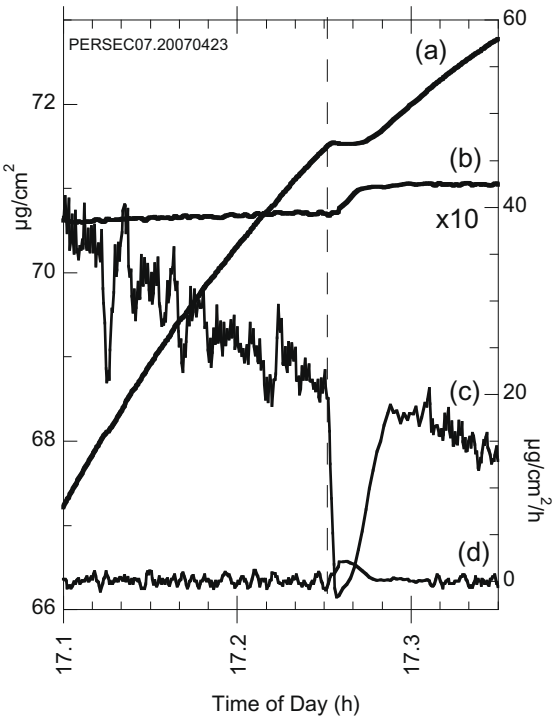

Fig. 2. Curve (a) shows the rise in mass on lower QMB during lithium evaporation interrupted by a deuterium gas-only pulse. In contrast the upper QMB (b) which is shadowed from the evaporator shows a small rise during the gas pulse. The data for (b) has been multiplied ×10 and offset by −155 μg/cm^2 to bring the curves to the same frame. Curves (c) and (d) show the respective deposition rates. The LiTER temperature cooled from 671 °C at 17.1 h to 657 °C at 17.35 h.

NSTX discharges are typically followed by intershot HeGDC initiated by two anodes at the Bay G and K midplane with the vessel wall being the cathode. The glow discharge helium pressure is 2.5 mtorr (0.33 Pa) with 450 V and 1.5 A per electrode [10]. Fig. 3 shows the interruption of deposition on the lower QMB from the time of the introduction of helium until after the HeGDC is terminated and the He pumped out. The Li–He mean free path was calculated using the same approach as for deuterium with the diffusion cross sections from Ref. [21]. The mean free path of neutral lithium at 627 °C in 2.5 mtorr of helium at 27 °C was calculated to be 2.7 cm. This is consistent with the interruption of deposition on the lower QMB and slight rise in upper QMB before and after, but not during the HeGDC. The additional factor in the glow discharge is ionization of Li and its drift in the electric field to tiles in the vicinity of the evaporator. Heavy lithium deposition was observed on these tiles after the end of the campaign when the vessel was opened for inspection. The momentum transfer cross sections of Ref. [22] were used to calculate the mean free path of Li^+. At 627 °C in 2.5 mtorr of helium at 27 °C it is 0.50 cm, somewhat smaller than the mean free path of neutral lithium because of the stronger interaction of Li^+ and He. The evaporated lithium undergoes diffusive transport in helium until it is ionized, and then a diffusive drift back to the wall where it formed a thick coating.

3. Mechanical stability of thick films

The unprecedented >400 s duration anticipated for ITER plasmas will facilitate the generation of thick codeposits. Quartz microbalances can offer information on the mechanical stability of deposits in contemporary tokomaks that is otherwise difficult to diagnose *in-situ*. Previously a sharp decrease in mass over seven discharges was reported on NSTX QMBs in a different geometry [8].

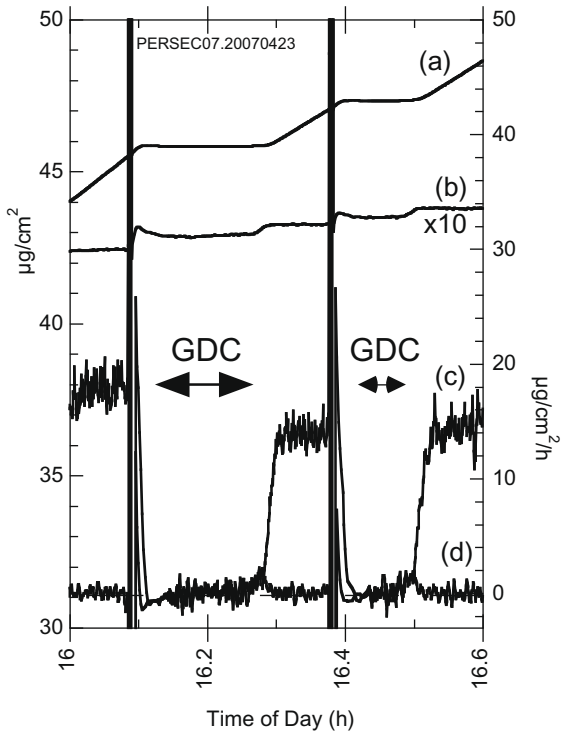

Fig. 3. Curve (a) shows the rise in mass on lower QMB during lithium evaporation interrupted by helium glow discharge cleaning (GDC). The upper QMB (b) that is shadowed from the evaporator shows a small rise during the gas pumpout after GDC. The data for (b) has been multiplied ×10 and offset by −180 μg/cm² to bring the curves to the same frame. Curves (c) and (d) show the respective deposition rates. The large vertical excursions are due to electrical pickup at the plasma discharge. The LiTER temperature was 620 °C at 16 h increasing to 635 °C at 16.6 h.

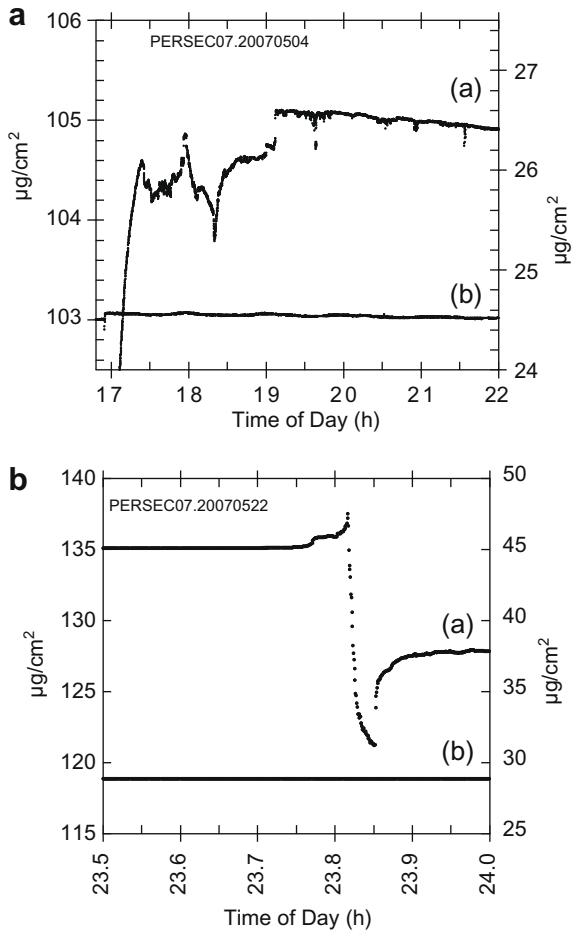

Fig. 5. Fluctuations in the apparent mass on the upper and lower QMBs after lithium evaporation. Curve (a) is the lower QMB, and (b) the upper QMB (scale on right, without multiplier or offset). These are interpreted as relaxation of mechanical stress and/or flaking of the deposits.

Fig. 4 shows a scanning electron microscope image of the deposit on the bay I midplane QMB crystal. A layered inhomogeneous structure with cracks is evident. Fig. 5(a) shows the apparent mass on the Bay H upper and lower QMBs recorded after the day's plasma operations with the lithium deposition rate decreasing as the evaporator cooled down. The areal mass density of the lower QMB, as derived from the crystal frequency, fluctuates by ∼1 μg/cm², but there is no external source that can account for the mass change. In contrast, the frequency of the upper QMB, shadowed from the lithium evaporator did not exhibit these fluctuations. The upper QMB accumulated a total of 36 μg/cm² compared to 196 μg/cm² on the lower QMB suggesting that the film thickness is a factor. Fig. 5(b) shows an even more precipitous drop in apparent mass of 15 μg/cm² in the lower QMB at a time close to midnight with no operational activity. The drop was followed by a partial recovery.

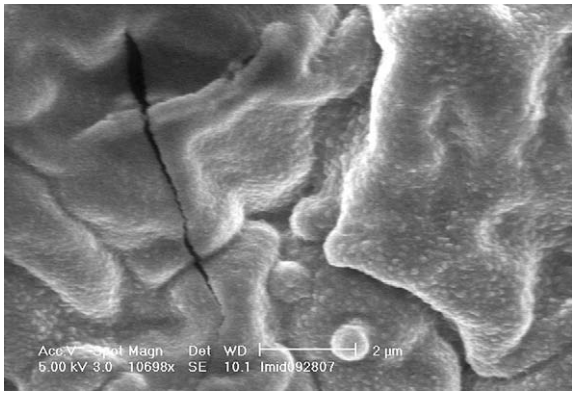

Fig. 4. Scanning electron microscope image of deposit on Bay I crystal. Scale bar is 2 microns.

In order to change the crystal oscillation frequency the deposited mass must be mechanically coupled to the quartz crystal. Material such as dust that is not mechanically attached to the crystal does not change its frequency [23]. We interpret the fluctuations in crystal frequency and in the derived mass as being due to the relaxation of mechanical stress and possibly flaking or peeling of the thick deposited film. Since the lower crystal faces upward it seems unlikely that the material has fallen off, but remains on the crystal without being mechanically coupled to it.

Projections of thick carbonaceous deposits and the associated tritium retention in ITER with a carbon divertor target plate have led to the proposal to exclude carbon PFCs from ITER's DT operations. However tritium will still be codeposited with beryllium. Over each operational day of fifteen 400 s duration plasma pulses a layer up to 6–12 microns of codeposited tritium with beryllium is projected to accumulate on the ITER baffle (estimated growth rate of order 1–2 nm/s) [24,25]. Strong thermal cycling and mechanical vibrations are expected. Whether the accumulating BeT layer remains attached to the baffle, or flakes and falls down into hard-to-access areas is a key consideration in the design and implementation of measures to remove tritium and control the ITER tritium inventory.

In summary, lithium deposition in NSTX has been measured by QMBs. Changes in the transport of lithium from the evaporator to the plasma facing components due to neutral gas collisions and

glow discharges have been measured and compared to calculations of the mean free path. Evidence for mechanical instability in the attachment of thick films has been presented.

Acknowledgments

The authors thank T. Holoman, D. Labrie, P. Roney, H. Schneider, J. Timberlake and the NSTX team for technical assistance. This work was funded by US DOE Contract Nos. DE-AC02-76CH0307 and DE-AC05-00OR22725.

References

[1] R. Kaita et al., J. Nucl. Mater. 363–365 (2007) 1231.
[2] J.E. Menard et al., Nucl. Fus. 47 (2007) S645.
[3] H.W. Kugel et al., Phys. Plasmas 15 (2008) 056118.
[4] H.W. Kugel et al., Evaporated lithium surface coatings in NSTX, these Proceedings.
[5] W.R. Wampler et al., J. Nucl. Mater. 390–391 (2009) 1009.
[6] J.P. Allain et al., Lithiated graphite as a hydrogen-pumping surface for improved plasma performance, these Proceedings, doi:10.1016/j.jnucmat.2009.01.242.
[7] C.S. Lasnier et al., Fus. Sci. Technol. 53 (2008) 640.
[8] C.H. Skinner et al., J. Nucl. Mater. 337–339 (2005) 129.
[9] C.H. Skinner et al., J. Nucl. Mater. 363–365 (2007) 247.
[10] C.H. Skinner et al., Nucl. Fus. 42 (2002) 329.
[11] Y. Tanaka et al., Phys. Plasmas 14 (2007) 052504.
[12] J.P. Coad et al., J. Nucl. Mater. 290–293 (2001) 224.
[13] P. Andrew et al., Fus. Eng. Des. 47 (1999) 233.
[14] C.H. Skinner et al., Nucl. Fus. 39 (1999) 1081.
[15] T.I. Ganbosi, Gaskinetic Theory, Cambridge University Press, 1994.
[16] R.A. Kendall, E. Apra, D.E. Bernholdt, et al., Comput. Phys. Commn. 128 (2000) 260.
[17] A. Boutalib, F.X. Gadea, J. Chem. Phys. 97 (1992) 1144.
[18] P.S. Krstic, D.R. Schultz, Phys. Rev. A 60 (1999) 2118.
[19] P.S. Krstic, D.R. Schultz, J. Phys. B 32 (1999) 2415.
[20] R. Côté, M.J. Jamieson, Z.-C. Yan, N. Geum, G.-H. Jeung, A. Dalgarno, Phys. Rev. Lett. 84 (2000) 2806.
[21] W.A. Hamel, J.E.M. Havenkort, H.G.C. Werij, J.P. Woerdman, J. Phys. B 19 (1986) 4127.
[22] M.T. Elford, I. Roeggen, H.R. Skullerud, J. Phys. B 32 (1999) 1873.
[23] A. Bader et al., Rev. Sci. Instrum. 75 (2004) 370.
[24] J.N. Brooks, J.P. Allain, T.D. Rognlien, Phys. Plasmas 13 (2006) 122502.
[25] J.N. Brooks, Personal Communication, 2008.